JOURNAL OF MATERIALS SCIENCE 29 (1994) 4535–4544

SIMS, EDX, EELS, AES, XPS study of interphases in nicalon fibre–LAS glass matrix composites

Part II *Chemistry of the interphases*

C. PONTHIEU*, C. MARHIC
Physique des Matériaux, Centre National de la Recherche Scientifique, 92 195 Meudon-cedex, France

M. LANCIN†
Physique Cristalline, Institut des Materiaux de Nantes, 44072 Nantes-cedex 03, France

N. HERBOTS
Department of Material Science and Engineering, Massachusetts Institute of Technology, MA 02139, USA

Auger electron (AES), electron energy loss (EELS) and X-ray photoelectron spectroscopy (XPS) were used to identify the reaction products at the fibre–matrix interface in SiC nicalon fibre–LAS (Li_2O, Al_2O_3, SiO_2) or LAS + Nb_2O_5 glass matrix composites. Chemical bonding of the different elements was investigated by AES using sputter-depth profiling on fibres extracted from two matrices by etching in hydrofluoric acid. The chemistry of the silicium was studied by EELS in nicalon–LAS + Nb_2O_5 composite cross-sections. XPS was performed on fibres extracted from the nicalon–LAS + Nb_2O_5 composite to confirm EELS and AES results. These investigations show that in both composites the reaction scale at the fibre–matrix interface consists of a carbon layer next to the matrix and of a silicate phase rich in oxygen which contains carbon, probably in the form of a silicon oxycarbide, and which is located between the carbon layer and the fibre core.

1. Introduction

The compositional characteristics of two interphases previously identified by high resolution transmission electron microscopy (HRTEM) [1] in SiC nicalon fibre Li_2O, Al_2O_3, SiO_2–LAS glass matrix composites were described in Part I of this article. The phase composition of the layer next to the matrix, the carbon layer (CL), is well established and confirms previous results [2–5]. The analyses suggest that the transition region (TR), which lies between the carbon layer and the fibre core, contains a silicate phase rich in oxygen, and the amount of this phase is highest next to the CL.

The aim of this paper is to identify this oxygen-rich phase formed by fibre–matrix reaction. The interphases were thus analysed using techniques which could reveal the chemical bonding of the elements detected in the TR. The chemistry of the interfacial layer was investigated by Auger electron spectroscopy (AES). AES has rather good lateral resolution ($L < 50$ nm) and good sensitivity to the chemical states of the silicon, carbon and oxygen which are found in the interphases. The AES analyses were complemented by a study of Si bonding at the CL–TR interface by electron energy loss spectroscopy (EELS) and by X-rays photoelectron spectroscopy (XPS). EELS analysis has excellent spatial resolution (≈ 6 nm), but may be influenced by the oxidation of thin foils. XPS has poorer spatial resolution than AES or EELS, but results in more accurate chemical information than AES and, in the case of the TR, than EELS.

2. Samples

EELS analyses were performed on cross-sections of nicalon–LAS + Nb_2O_5 composite, and the AES and XPS analyses on fibres extracted from nicalon–LAS and/or LAS + Nb_2O_5 as described in Part I. Pure α-SiC, pure SiO_2 and the core of a nicalon fibre were also characterized by AES and EELS to calibrate the data.

3. AES analysis of the near surface of extracted fibres

The purpose of the Auger analysis is to characterize the chemical states of the silicon, carbon and oxygen in the interfacial region as a function of depth.

* Permanent address: Saint Gobain Recherche, 28 Quai Lucien Lefranc, BP 135, 93 303 Aubervilliers-cedex, France.
† Author to whom correspondence should be sent.

0022–2461

3.1. Experimental parameters

Auger electron spectroscopy was carried out on a Perkin Elmer 660 instrument. A 3 keV primary electron beam current of 30 ± 5 nA was used for Auger electron excitation. The relative energy resolution of the spectrometer was 0.6%. As for the secondary ion mass spectroscopy (SIMS) analysis, the interfacial region was characterized by sputter profiling the surface of extracted fibres. The sputtering was done with an Ar^+ ion beam whose energy was 3 keV and whose current density was 45 mA cm^{-2}. An AES analysis was performed at sputtering intervals of 1 min. The diameter of the analysed region was about 100 nm.

3.2. Choice of Auger transitions

To characterize the silicon, the LMM Auger transition was selected. Several reasons justify this choice. Firstly, the LMM transition signal of Si bonded in SiO_2 is located at about 76 eV, while the LMM transition signal of Si in pure Si is found at about 92 eV. This means that SiO_2 can be easily distinguished from unoxidized Si. Secondly, the resolution of the spectrometer, proportional to the energy, is better at lower energies (0.6 eV at 92 eV). Finally, the relative sensitivity factor for Si is much larger for the LMM transition (0.35) than for the KLL transition (0.025). For carbon and oxygen, the only available transition is the KLL. The KLL transition for carbon and oxygen is located at about 272 and 510 eV, respectively. The energy resolution of the spectrometer for each transition is given in Table I.

3.3. Calibration references

The silicon and carbon transitions were studied in an α-SiC standard, used as a reference during the SIMS analysis. The Si–LMM and the C–KLL Auger transitions were measured after 1, 2, 3, 4 and 5 min sputtering. The transitions do not change during sputtering (Fig. 1). Therefore, it can be assumed that Ar^+ sputtering does not induce any chemical modification in the SiC phase. The characteristics of the Si and C transitions are given in Table I. Note that the Si–LMM transition is observed at 93.1 eV in SiC.

The Si, C and O transitions were characterized in the core of a nicalon fibre (Fig. 2). The main characteristics of these transitions are shown in Table I. As in SiC, no changes in the transitions were observed during sputtering. Sputtering does not induce detectable chemical modifications of the nicalon fibre. It is important to note that a Si–LMM transition is observed at 92.7 eV, but that no signal is detected at 76 eV. The contribution of a few per cent SiO_2 present in the nicalon fibre is not detected in the Si line, thereby showing that there is a threshold to AES sensitivity in the presence of SiO_2.

TABLE I Characteristics of the AES peaks in α-SiC and in the 202 nicalon fibre. The resolution of the spectrometer for the energies characteristic of the different transitions are indicated in the table.

α–SiC	Si–LMM transition	$E_{Si} = 93.1 \pm 0.5$ eV
	(Fig. 1)	$W_{Si} = 5.3 \pm 0.5$ eV
	C–KLL transition	$E_C = 275 \pm 1.6$ eV
	(Fig. 1)	$W_C = 8.4 \pm 1.6$ eV
Nicalon fibre core	Si–LMM transition	$E_{Si} = 92.7 \pm 0.5$ eV
	(Fig. 2)	$W_{Si} = 6.6 \pm 0.5$ eV
	C–KLL transition	$E_C = 274 \pm 1.6$ eV
	(Fig. 2)	$W_C = 8.7 \pm 1.6$ eV
	O–KLL transition	$E_O^1 = 511 \pm 3$ eV
	(Fig. 2)	$E_O^2 = 491 \pm 3$ eV

The superposition of Si transitions obtained in α-SiC and in the nicalon fibre (Fig. 2a) shows that the left part of the Si transition is less abrupt in the nicalon fibre than in pure SiC and that its energy position is slightly lower, 92.7 instead of 93.1 eV. The nicalon fibre not only contains SiC ($\approx$ 45 mol % [6]), but also a significant amount of SiO_xC_y ($\approx$ 20 mol % [6]). Therefore, it can be assumed that these changes in the Si–LMM Auger transition line shape and energy position are due to SiO_xC_y, which is contained in the nicalon fibre.

Unlike the Si transition, the shape and energy position of the C–KLL transition of pure α-SiC and of the Nicalon fibre are within the resolution of the spectrometer (Table I).

3.4. Auger characterization of the transition region

3.4.1. Chemical state of the silicon

The silicon transition line shape and energy position were studied as a function of depth in fibres extracted from the nicalon–LAS and the nicalon–LAS + Nb_2O_5 composites. As an illustration, Fig. 3 shows the Si–LMM transition after increasing sputtering times for a fibre extracted from the nicalon–LAS. The Si–LMM transition is always observed at about 92 eV. In both composites, a signal located at 76 eV which is the expected energy position for SiO_2 was never observed in the TR. Thus, as in the fibre core, the SiO_2 content in the TR does not exceed a few per cent.

In all samples, the shape and energy position of the Si–LMM transition change significantly throughout the TR before becoming stable in the fibre core. The left side of the transition becomes more abrupt and the energy position of the transition increases. In order to quantify this evolution, a reference transition, Pref, was chosen in the fibre core. As shown in Fig. 4a, the shift (S) in the energy width of the LMM transition at the half-maximum, between the left side of Pref and the left side of each Si–LMM transition was measured. S and the absolute energy position (E) versus the sputter time (t) (Figs 4b, c and 5) were then correlated. The change of S and E are both significant with respect to sensitivity of the measurement. For the fibres extracted from LAS and from LAS + Nb_2O_5, the maximum value of S is 1.5 and 1.4 eV, and the change in the energy position is about 1 and 1.1 eV, respectively; while the resolution of the spectrometer at 92 eV is 0.5 eV.

Auger analysis reveals significant evolution of the Si transition line shape and energy position throughout the TR. The reference studies performed on pure α-SiC and on the nicalon fibre suggest that this evolution is due to an increase in the SiO_xC_y content and a decrease in the SiC content in the TR from the fibre

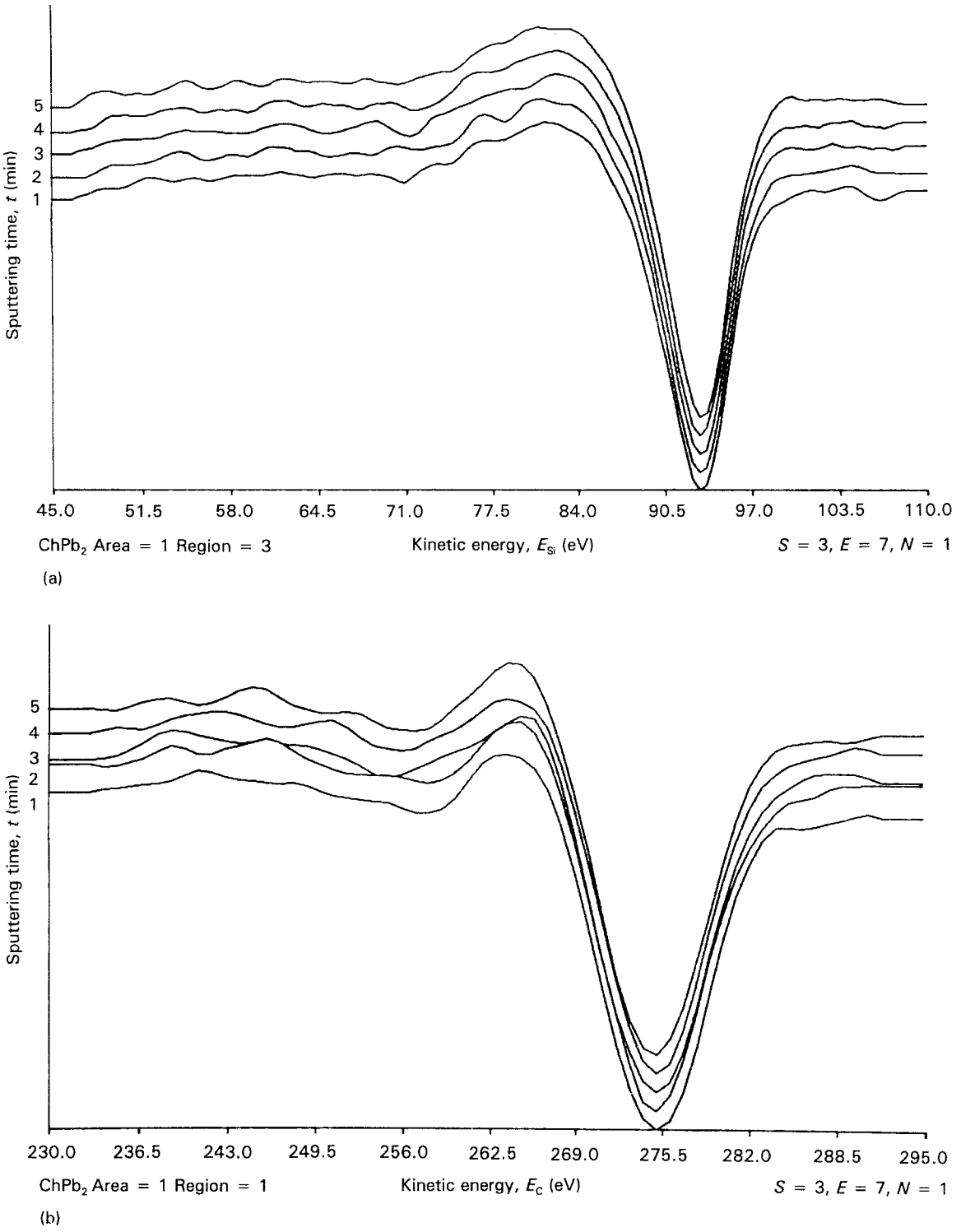

Figure 1 (a) Si–LMM, and (b) C–KLL Auger transitions obtained in α-SiC after 1, 2, 3, 4 and 5 min sputtering. The curves are translated parallel to the *y*-axis, to be compared.

core to the carbon layer (CL). These observations by AES are consistent with the SIMS and energy dispersive spectroscopy (EDX) profiles (see Part I), which revealed an increase in the oxygen content of the TR from the fibre core to the carbon layer. They are also consistent with the HRTEM images [1], which show a gradual decrease in the number of SiC grains from the fibre core to the CL.

3.4.2. Chemical state of the carbon

The C–KLL carbon transition was profiled from the CL to the fibre core (Fig. 6). As for the silicon signal, in all samples evolution of the line shape of the carbon transition was observed. The surface plasma transition, located at about 250 eV, which is detected throughout the carbon layer, disappears and the width (W) at half-maximum of the C–KLL transition decreases as sputtering time increases. W and the energy position of the transition were plotted versus the sputter time (t) for fibres extracted from both composites (Figs 7 and 8). The changes in the energy positions observed in all the fibres (< 1.6 eV) are not significant, since the resolution of the spectrometer is 1.6 eV at the energy of the carbon transition. On the

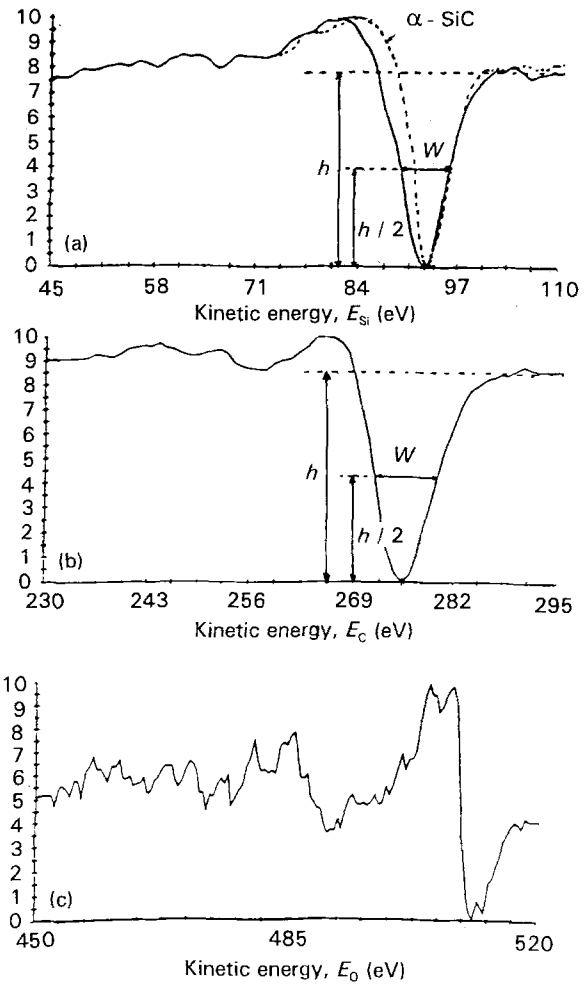

Figure 2 (a) Si–LMM, (b) C–KLL and (c) O–KLL Auger transitions obtained in the core of a nicalon fibre. In Fig. 2a the Si–LMM transition of the α-SiC is superimposed with a dashed line.

contrary, the broadening of the C–KLL transition from the fibre core to the CL, which is equal to 1.8 and 2.8 eV in the fibres extracted from the LAS and LAS + Nb_2O_5, respectively, is significantly higher than the resolution of the spectrometer.

In both composites, the broadening of the C–KLL transition from the fibre to the CL indicates a chemical change throughout the TR. The width of the transition changes progressively from its value in SiC. This result suggests that the amount of SiC, which is one of the three major components of nicalon, decreases from the fibre core to the CL. This conclusion agrees with ones derived from analysis of the Auger Si–LMM transition. It is also consistent with EDX and SIMS analyses, and with HRTEM results [1].

3.4.3. Chemical state of the oxygen

No significant evolution of line shape and energy position of the oxygen transition is observed during the depth profiling of the fibres (Fig. 9). The resolution of the spectrometer at 500 eV is rather low (3 eV). However, if a change in the Auger transition indicates a change in chemistry, the opposite is not necessarily true. Therefore, no conclusions can be drawn concerning the chemical state of the oxygen in the TR.

4. EELS analysis of the composite interphase

The purpose of the EELS analysis was to obtain additional chemical information concerning the oxygen-rich phase formed during fibre–matrix reaction. From the AES results it can be assumed that the chemical state of the silicon in the TR is similar in both composites. The TR in the nicalon–LAS + Nb_2O_5 was thus analysed, because it was larger in this composite than in the nicalon–LAS (230 nm versus 30 nm). The changes in the Si–LMM transition line shape and energy position showed that the amount of the phase rich in oxygen is highest at the CL–TR interface. The chemistry of this phase at this interface was thus studied. The Si–$L_{2,3}$ edge was also studied in the α-SiC and SiO_2 standards and in the fibre core.

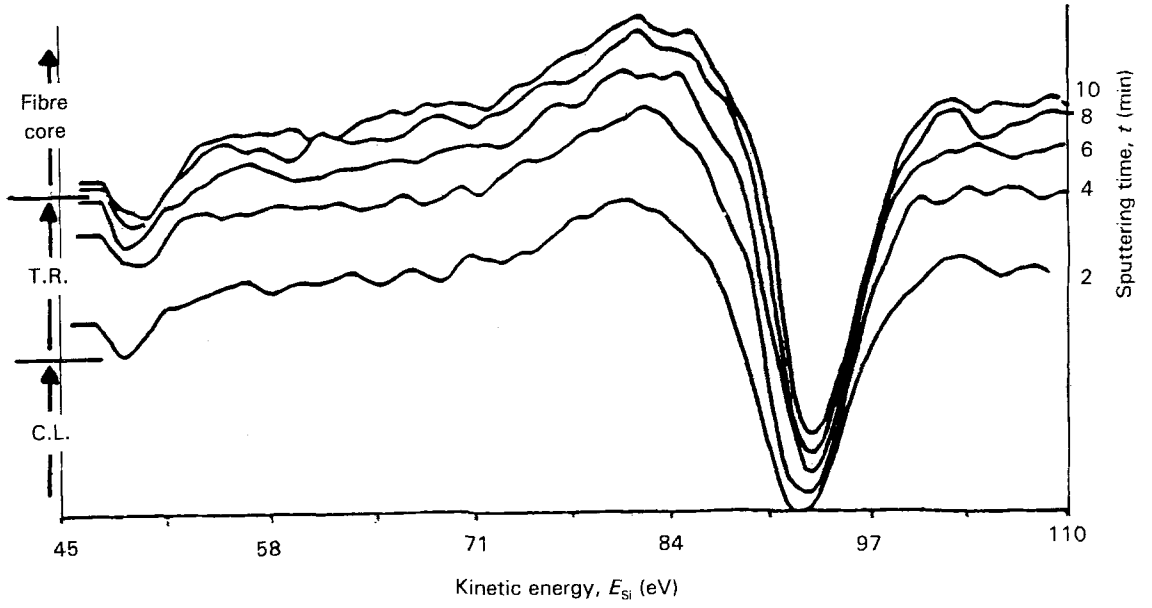

Figure 3 Fibres extracted from the LAS matrix composite. The AES Si–LMM curves obtained after increasing sputtering times are translated parallel to the *y*-axis.

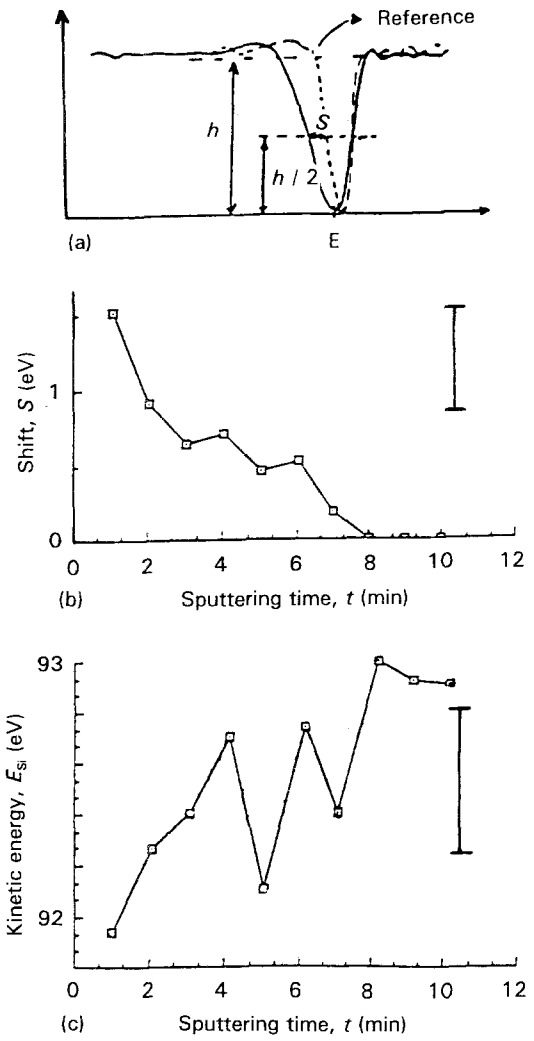

Figure 4 Changes in Si–LMM transition peak characteristics during the sputtering of fibres extracted from the LAS matrix composites. (a) definition of the shift, S; (b) and (c) variation versus the sputtering time, t, of S and of E_{Si}, respectively. The bar indicates the energy resolution.

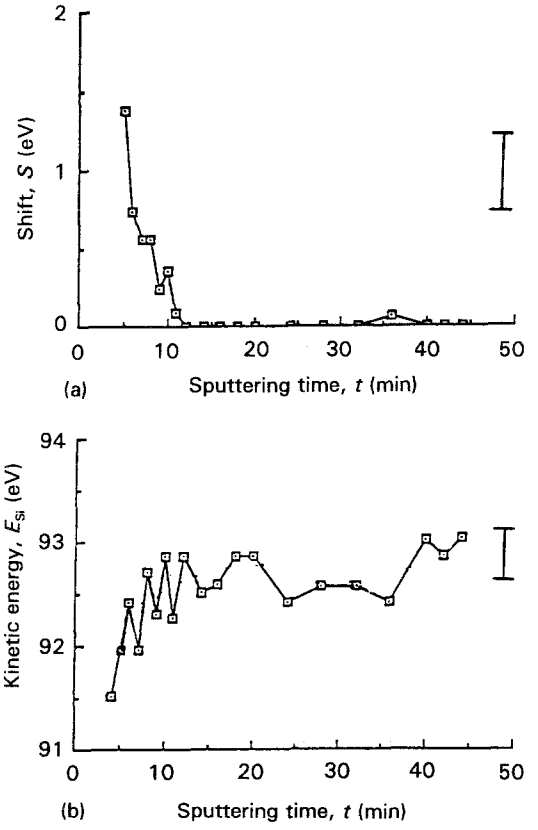

Figure 5 Changes in Si–LMM transition peak characteristics during the sputtering of fibres extracted from the LAS + Nb_2O_5 matrix composites. (a) and (b) variation versus the sputtering time, t, of S and of E_{Si}, respectively. The bar indicates the energy resolution.

4.1. Experimental procedure

The analyses were done using a Jeol 2000 FX equipped with a parallel EELS detector. The analyses were realised at 160 kV, in diffraction mode. The samples were fixed in a Gatan holder cooled at nitrogen temperature to avoid contamination. The Si–$L_{2,3}$ edges were collected using a sensitivity of 0.2 or 0.3 eV per channel. The thinness of the foils was checked while collecting the low energy losses. The analyses were performed in the TR next to the CL–TR interface, where a maximum in the oxygen content was detected by EDX using a 6 nm probe size. Analyses were also performed in the core of the analysed fibres. SIMS have shown that the interdiffusion fibre–matrix does not modify the composition of the fibre core. Due to the fibre microstructure and composition (cf. Part I) a 10 nm probe size was used, and it was checked that the characteristics of the Si–$L_{2,3}$ edge were independent of the probe location.

4.2. Calibration references

The Si–$L_{2,3}$ threshold energy and edge structure were characterized in α-SiC and in SiO_2 standards (Fig. 10a, b). The SiO_2 spectrum is in excellent agreement with the reference published in the Gatan library.

The Si–$L_{2,3}$ edge obtained in the fibre core is shown in Fig. 10c. The threshold is observed at 103 eV, as in SiC, but the edge exhibits structures at 108.5 and 116.3 eV which are not observed in SiC. These two structures are also found in SiO_2. However, AES and XPS demonstrate that the fibre contains only a small amount of SiO_2 (a few per cent) and about 20 mol % of another phase identified as SiO_xC_y by Porte and Sartre [6] and Lipowitz *et al.* [8]. This means that the structures at 108.5 and 116.3 eV are an indication of oxidized silicon, but they cannot discriminate between Si in SiO_2 or in SiO_xC_y.

4.3. Chemistry of the silicium in the TR interphase

An Si–$L_{2,3}$ edge obtained in the TR next to the CL is shown in Fig. 10d. It is clear that the spectrum is completely different from the edge obtained in the fibre core. EELS analysis thus confirms the compositional change revealed by SIMS, EDX and AES.

The Si–$L_{2,3}$ edge in the TR is very similar to the edge in SiO_2. The only clear difference is the relative height of the structures at 108.5 and 130 eV. It is known that convolution of the low energy losses with the studied edge results in similar effects in thick samples [7]. Such an artifact cannot account for the observed structure because the spectrum was collected

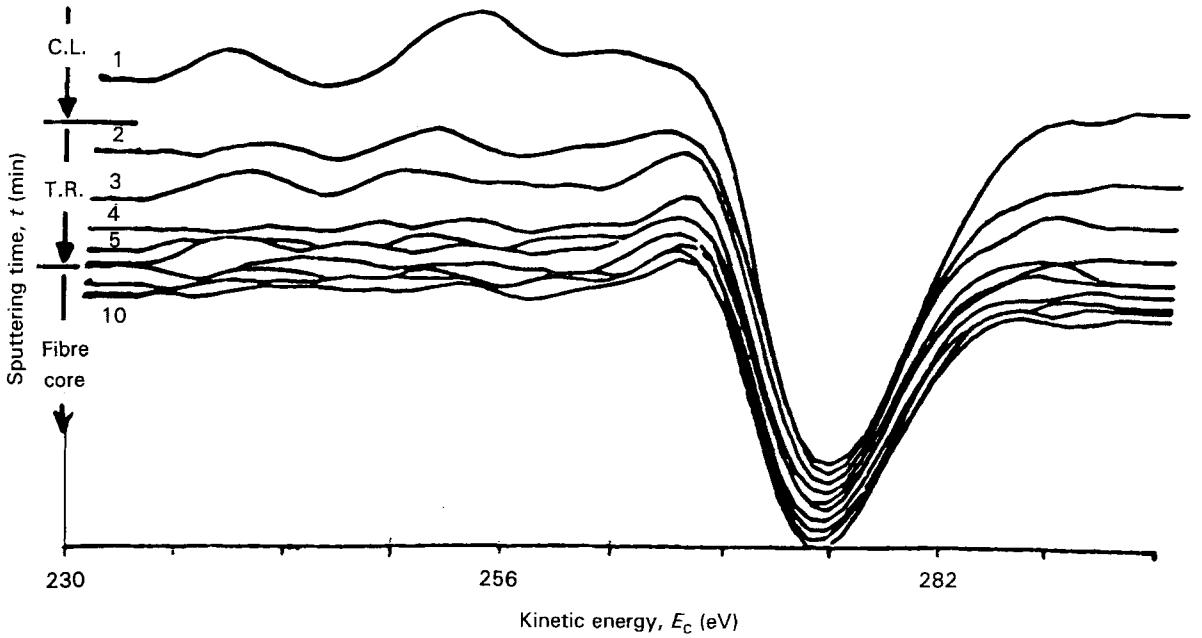

Figure 6 Fibres extracted from the LAS matrix composite. The AES C–KLL transitions obtained after increasing sputtering times are translated parallel to the *y*-axis.

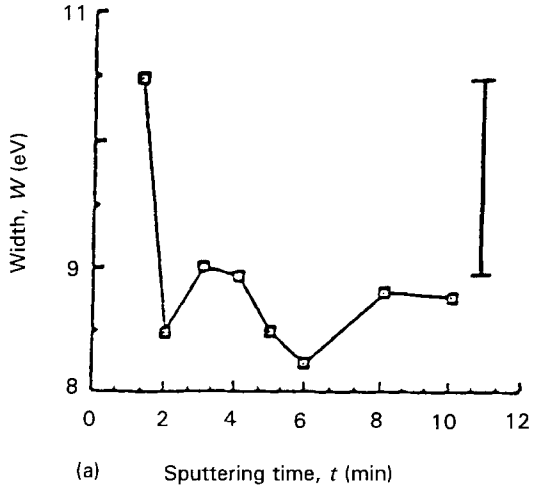

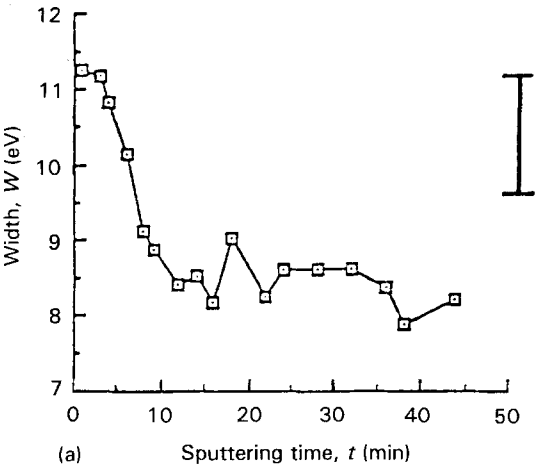

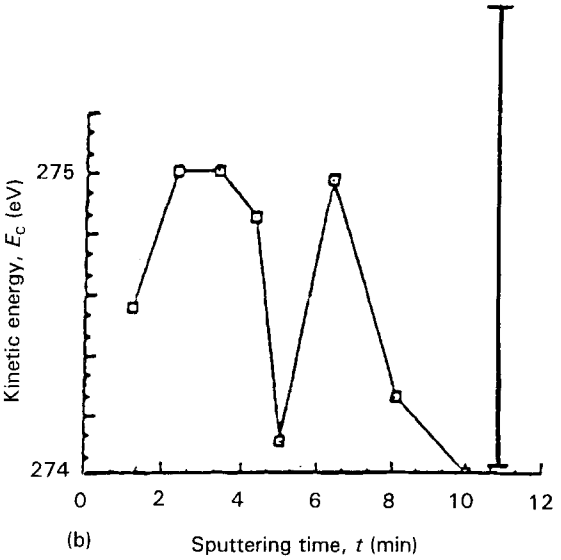

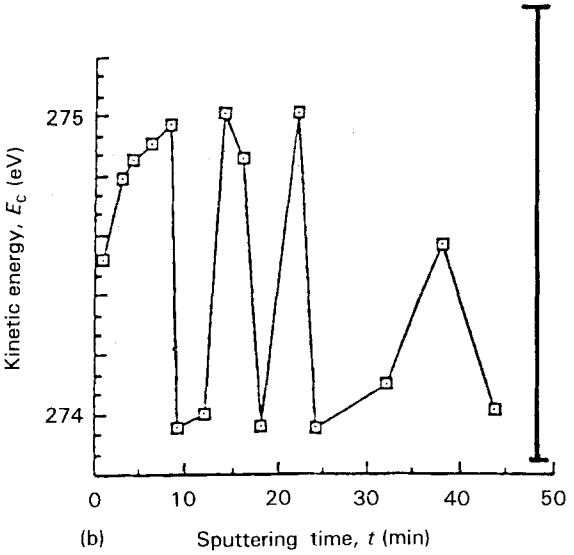

Figure 7 Changes in C–KLL Auger transition characteristics during the sputtering of fibres extracted from the LAS matrix composite. (a) and (b) variation versus the sputtering time, *t*, of *W* and of E_C, respectively. The bar indicates the energy resolution.

Figure 8 Changes in C–KLL Auger transition characteristics during the sputtering of fibres extracted from the LAS + Nb_2O_5 matrix composite. (a) and (b) variation versus the sputtering time, *t*, of *W* and of E_C, respectively. The bar indicates the energy resolution.

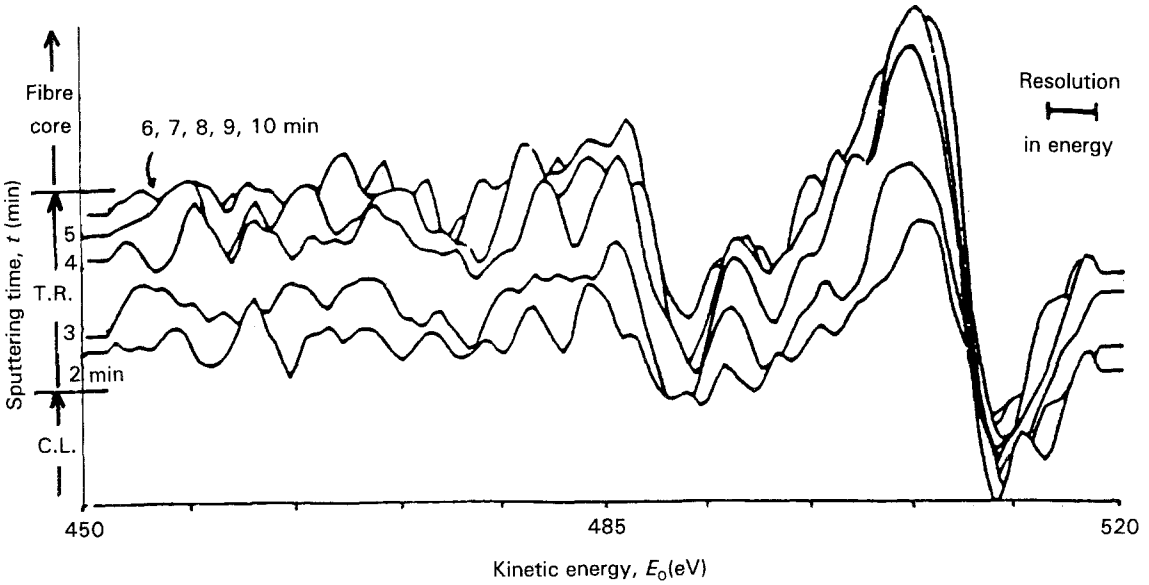

Figure 9 Fibres extracted from the LAS matrix composite. The O–KLL Auger curves obtained after increasing sputtering times are translated parallel to the *y*-axis.

in a thin area, as indicated by the single bulk plasmon peak (Fig. 10e).

The energy of the plasmon peak which has the same value as that in SiO_2 is not discussed for the two following reasons. Firstly, the same energy may correspond to distinct phases. Secondly, the volume involved in the collective excitation of the valence electrons is greater than the volume crossed by the electron beam. The analysis is thus influenced by the surroundings and particularly by the CL.

The Si–$L_{2,3}$ edge is now considered. Artifacts being excluded, it can be concluded that the TR spectrum does not correspond to pure SiO_2. From the HRTEM observations, it is clear that the density of SiC grains in the analysed area is smaller than in the fibre, but likely not equal to zero. The TR spectrum could be described as a convolution of the SiO_2 and SiC spectra, the SiO_2 content being predominant. As this assumption contradicts the AES results, it cannot be used. Moreover, analysis of the nicalon fibre proves that the structures at 108 and 115 eV are also found in SiO_xC_y. To be consistent with the AES results, which eliminate the possibility of having SiO_2, the TR spectrum may be attributed to SiO_xC_y. This assumption agrees with the conclusion derived from evolution throughout the TR of the line shape and energy position of the Auger Si–LMM transition.

5. XPS analysis

The purpose of the analysis is to complement AES and EELS results and thus to identify the oxygen-rich phase formed by fibre–matrix reaction. It was necessary to choose a method very sensitive to chemical bonding. XPS was selected because it provides information on the chemical state of the elements more precisely than AES does. Difficulties were encountered due to the fact that XPS lateral resolution is much larger than the fibre diameter (150 mm versus 15 mm). However, by using the AES analysis results, and a specific experimental procedure described below, it is possible to identify the chemical state of the silicium in the TR next to the CL.

5.1. Experimental parameters

The XPS analysis was carried out on a XSAM800 Kratos analytical spectrometer. The sample was irradiated by an Mg Ka line whose energy was 12 53,6 eV. The size of the analysed area was equal to a few mm^2. Therefore, the sample was made of a bundle of fibres which covered the surface of the sample holder.

The transition region (TR) is located between the carbon layer and the fibre core. To obtain information concerning this region, the carbon layer must be removed. This was done with an Ar^+ ion beam whose energy was 2.5 keV. As previously shown by AES, such sputtering does not induce any chemical modification of SiC, nor of the fibre, and thus of the SiO_xC_y contained in the fibre. Moreover, the chemistry of the TR next to the CL is discussed, that is to say at the beginning of the sputtering of the TR. Modification of the chemistry of the analysed TR is thus unlikely, and the detected photoemission is characteristic of the TR.

Due to the geometry of the sample, the sputtering rate of the carbon layer was not uniform all around the fibres. Therefore, photoelectrons issued from the CL and TR were analysed simultaneously. However, the CL did not contain any significant amount of silicon, as shown by the EDX and AES analyses. As a consequence, the first Si photo electron signal which appeared in the depth profile was emitted from the CL–TR interface by the oxygen-rich phase to be identified.

5.2. XPS characterization of the near surface of the extracted fibre

After 6 h sputtering, no Si was detected on the layer being analysed. This layer contained 91% C and 9% O. It is clear from this result that the carbon

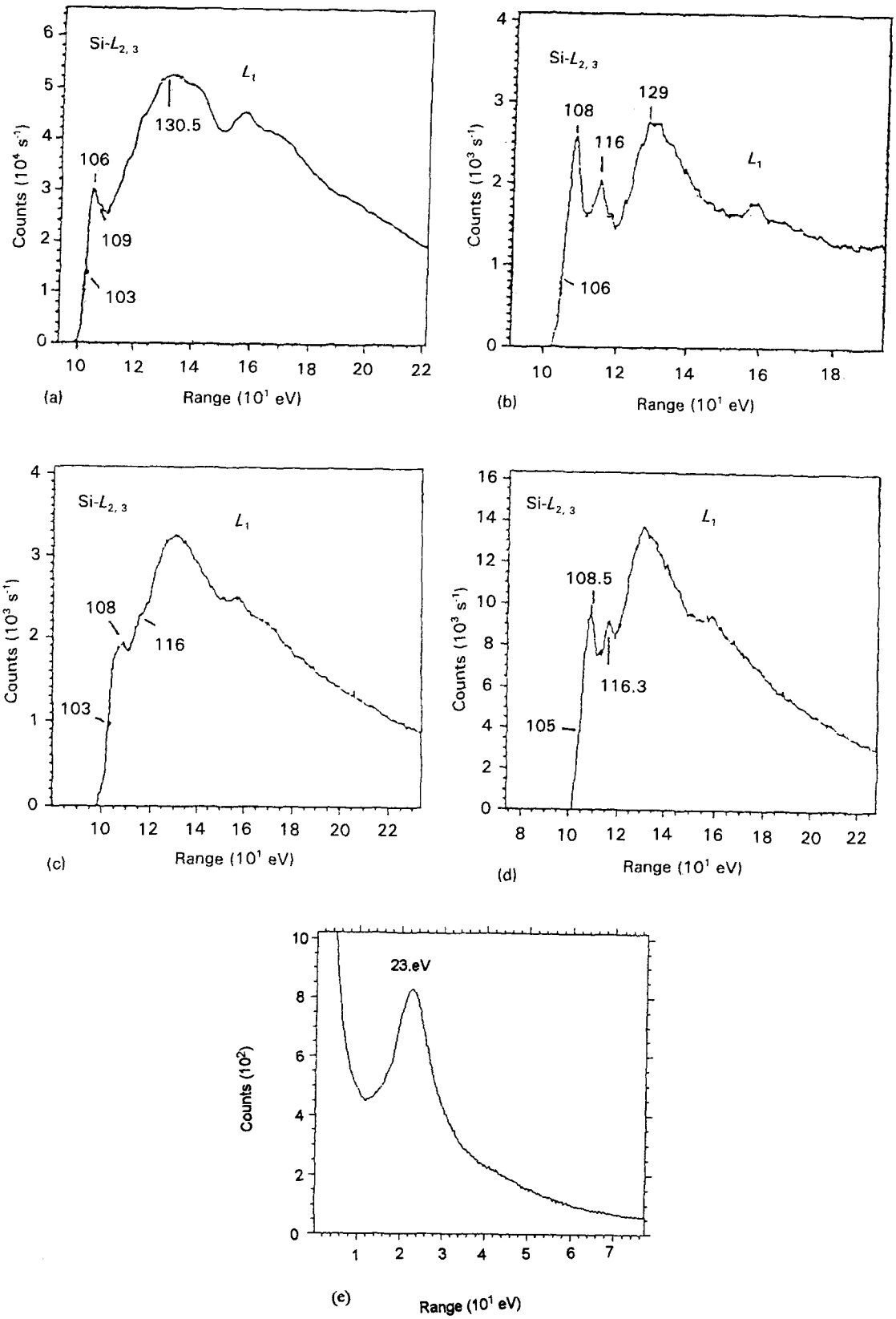

Figure 10 Si–$L_{2,3}$ edges and plasma peak obtained by PEELS (Parallel Electron Energy Loss Spectroscopy). The spectra are characteristic of the Si–$L_{2,3}$ edges in (a) α-SiC, (b) SiO_2, (c) the fibre core, and (d) the TR. The spectrum 10(e) shows the typical plasmon peak of the TR areas where the Si–$L_{2,3}$ edges were recorded.

covering the fibres was not completely removed. The high amount of oxygen can be attributed to oxidized fibre surfaces which were not yet eroded by the Ar^+ beam.

After 11 h sputtering, Si was detected on the area analysed. The atomic composition at that point of the profile was 78% C, 5% Si and 17% O. The energy position of the Si_{2P} photoemission and C_{1S} photoemission (Fig. 11) were, respectively, 101.7 and 284 eV.

The carbon 1S photoemission at 284.4 eV was still symmetric. No additional emission at 282.9 eV, typical of C bonded into SiC, was detected. The binding

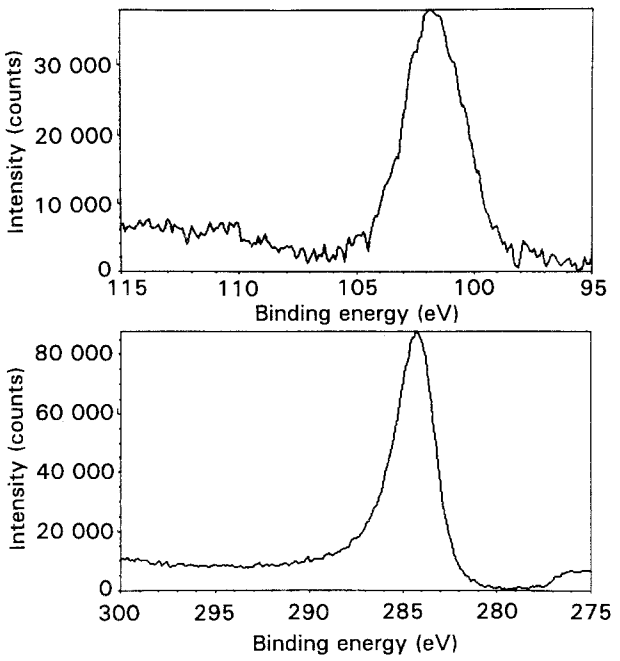

Figure 11 Photoemission obtained by XPS at the CL–TR interface. (a) Si_{2P}, and (b) C_{1S} photoemissions in fibres extracted from the nicalon–LAS + Nb_2O_5 composite.

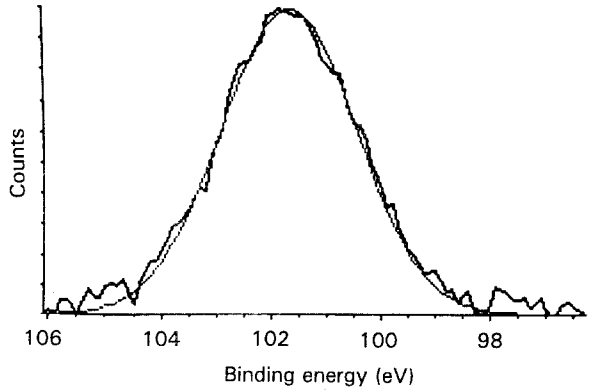

Figure 12 Fitting of the Si_{2P} XPS photoemission with one Gaussian curve.

energy of the carbon analysed, 284.4 eV, could be attributed either to free C or to SiO_xC_y as previously reported by Porte and Sartre [6].

The Si_{2P} photoemission was symmetrical and could be fitted by one single Gaussian curve (Fig. 12). Its energy position, 101.7 eV, is neither typical of Si in SiC (BE (Binding Energy) = 100.5 eV) nor of Si in SiO_2 (BE = 103.4 eV), but located right in-between them. The same intermediate photoemission, 101.5 eV, was reported in the nicalon fibre by Porte and Sartre [6] and attributed to a SiO_xC_y phase. Moreover, the energy of the carbon photoemission can be attributed to silicon oxycarbide as well. It can thus be assumed that Si_{2P} photoemission at the CL–TR interface originates from the same silicon oxycarbide phase.

6. Discussion

To characterize the phases formed by the fibre–matrix reaction, several techniques with complementary sensitivity and spatial resolution were used. Identification of the oxygen-rich phase was derived from cross-checking AES, EELS and XPS results. It is important to note that while the Auger analysis clearly eliminates the possibility of having the detected oxygen bonded into SiO_2 in the TR, it is not allowed to unambiguously establish the phase present. The evolution of the Si–LMM line shape and energy position throughout the TR suggests that only SiO_xC_y is the oxygen-rich phase formed by the fibre–matrix reaction. XPS demonstrates, by its superior energy resolution, that SiC and SiO_2 could not be a possibility for Si_{2P} photoemission, thereby leading to identification of silicon oxycarbide. EELS analysis, which cannot alone provide a firm conclusion, supports this conclusion. The XPS analysis also shows that silicon oxycarbide is the only silicon-containing phase detected next to the CL–TR interface. SiC, one of the two major components of Si photoemission in the nicalon fibre [6, 8] is no longer detectable. These results confirm and complete the conclusions derived from HRTEM observations and AES analysis.

The following conclusions can be derived from the whole study. The fibre–matrix reaction results in carbon and silicon oxycarbide phases. The silicon oxycarbide is located between the carbon and the fibre, its amount decreasing from the carbon to the fibre.

The silicon oxycarbide phase is formed by oxidation of SiC. Oxidation of SiC was known to result either in SiO_2 and volatile CO, or in volatile SiO and CO, depending on the temperature and oxygen pressure [8–12]. In the particular case of the nicalon fibre, two mechanisms were proposed but both resulted in the formation of SiO_2 + C [13, 14]. This models deal with thermodynamic equilibrium between SiC, SiO_2 and O_2. The results described in this paper contradict these models. The disagreement between the model and experimental results may be due to the specific microstructure of the nicalon fibre. The SiC grains are about 2 nm in diameter and are surrounded by carbon and SiO_xC_y. The activity of the SiC may be modified by this microstructure. This hypothesis is supported by another experimental result. A composite consisting of SiC particles, 15–20 nm in diameter, and of LAS + Nb_2O_5 glass matrix was hot-pressed under the same hot pressing conditions as nicalon–LAS + Nb_2O_5 [15]. At the periphery of the particles, HRTEM observations did not reveal any interphase. Thus, if an interphase exists, its width must be restricted to about 1 nm. That is to say, if oxidation of SiC occurs it is much more restricted than in the nicalon fibre.

Oxidation of the nicalon fibre by the LAS and the LAS + Nb_2O_5 glass matrices results in the same phases. The difference between the two composites is in the amount of the resulting phases, which itself derives from the oxidizing ability of the matrices. A kinetic analysis of the reaction in the two composites was done in order to describe better the fibre–matrix reaction. It will be discussed in a following paper.

7. Conclusion

By using a combination of several analytical techniques, SIMS, EDX, AES, EELS and XPS, better

knowledge of the interfacial region of nicalon fibres–LAS or LAS + Nb_2O_5 glass matrix composites, previously characterized by TEM and HRTEM, has been obtained. The fibre–matrix interaction, which occurs during hot pressing of the composites, results in two interphases: a carbon interphase next to the matrix and a "transition region", TR, between the carbon interphase and the fibre core. The well known NbC grains which edged the carbon in the LAS + Nb_2O_5 glass matrix were beyond the scope of this article. SIMS reveals that diffusion of the matrix elements into the fibre occurs far beyond the region where microstructural changes take place, TR, revealed by HRTEM.

In both composites, the features of the TR are similar. The TR is richer in oxygen and poorer in silicon and carbon than the fibre core. The chemistry of the silicon in the TR is different from that in the fibre core. The line shape and width of the Si–LMM Auger transition, the Si–$L_{2,3}$ EELS edge structure and the energy position of the Si_{2P} photoemission suggest that the TR is rich in a silicon oxycarbide phase. AES shows that the amount of SiC decreases, whereas the amount of SiO_xC_y increases in the TR from the fibre core to the carbon interphase. XPS reveals that silicon oxycarbide is the only silicon-containing phase at the CL–TR interface. SiO_xC_y is thus formed by oxidation of the SiC contained in the fibre by the matrix. The oxidation mechanism of SiC seems to be due to the specific microstructure of the nicalon fibre.

This paper also demonstrates how different techniques can be combined in a non-classical way to obtain chemical information about the interphases surrounding fibres of small diameter.

Acknowledgements

The authors thank Saint Gobain Recherche for the composites and for supplying the research grant of one of them, and DRET for financial support.

References

1. C. PONTHIEU, M. LANCIN and J. THIBAULT-DESSEAUX, *Phil. Mag.* **62** (1990) 605.
2. J. J. BRENNAN, *J. Phys. suppl.* **10 C5** (1988) 791.
3. R. F. COOPER and K. CHYUNG, *J. Mater. Sci.* **22** (1987) 3148.
4. D. H. GRANDE, J. F. MANDELL and K. C. C. HONG, *ibid.* **22** (1988) 311.
5. B. MEIER and G. GRATWHOL, *Fresenius Z Anal. Chem.* (1989) 388.
6. L. PORTE and A. SARTRE, *J. Mater. Sci.* **24** (1989) 271.
7. R. F. EGERTON, "Electron Energy loss Spectroscopy in the Electron Microscope" (Plenum, New York, 1985).
8. J. LIPOWITZ, H. A. FREEMAN, R. T. CHEN, E. R. PRACK, *Adv. Ceram. Mater.* **2** (1987) 121.
9. E. A. GULBRANSER and S. A. JANSSON, *Oxid. Met.* **4** (1972) 181.
10. D. W. McKEE and D. CHATTERJI, *J. Am. Ceram. Soc.* **71** (1988) 960.
11. L. U. OGBUJI, *J. Mater. Sci.* **16** (1981) 2753.
12. J. COSTELLO and R. E. TRESSLER, *J. Am. Ceram. Soc.* **69** (1986) 674.
13. R. F. COOPER and K. CHYUNG, *J. Mater. Sci.* **22** (1987) 3148.
14. P. M. BENSON, K. E. SPEAR and C. G. PENTANO, *Ceram. Eng. Sci. Proc.* **9** (1988) 663.
15. C. PONTHIEU, Thèse de l'Université Paris VI (1990)

Received 24 May
and accepted 10 November 1993